

Populus endo-glucanase 16 localizes to the cell walls of developing tissues

Hila Behar^{1,2} | Yaseen Mottiar³  | Rohan Chandrasekhar³ |
 Allegra Corelli Grappadelli⁴  | Markus Pauly⁴  | A. Lacey Samuels⁵  |
 Shawn D. Mansfield^{3,5} | Harry Brumer^{1,2,5,6} 

¹Michael Smith Laboratories, University of British Columbia, Vancouver, British Columbia, Canada

²Department of Biochemistry and Molecular Biology, University of British Columbia, Vancouver, British Columbia, Canada

³Department of Wood Science, University of British Columbia, Vancouver, British Columbia, Canada

⁴Institute for Plant Cell Biology and Biotechnology, Heinrich Heine University, Düsseldorf, Germany

⁵Department of Botany, University of British Columbia, Vancouver, British Columbia, Canada

⁶Department of Chemistry, University of British Columbia, Vancouver, British Columbia, Canada

Correspondence

Harry Brumer, Michael Smith Laboratories, University of British Columbia, 2185 East Mall, Vancouver, British Columbia, Canada, V6T 1Z1. Email: brumer@msl.ubc.ca

Funding information

Work at the University of British Columbia was supported by the Natural Sciences and Engineering Research Council of Canada (NSERC) Discovery Grants to H. Brumer (RGPIN 435223-13 and RGPIN 2018-03892), S.D. Mansfield (RGPIN 2017-04566), and A. L. Samuels (RGPIN 2019-04592). H. Behar was partially supported by the NSERC-CREATE/DFG-IRTG joint training program “PRoTECT: Plant Responses To Eliminate Critical Threats.” A.C. Grappadelli was funded by the Deutsche Forschungsgemeinschaft (DFG) graduate school program “Nextplant,” GRK2466/1. M. Pauly is funded by the Deutsche Forschungsgemeinschaft (DFG) under Germany’s Excellence Strategy—EXC 2048/1—Project ID No. 390686111.

Abstract

The hemicelluloses comprise a group of matrix glycans that interact with cellulose microfibrils in plant cell walls and play important roles in establishing wall architecture. The structures of hemicelluloses are determined by carbohydrate-active enzymes (CAZymes) that synthesize, integrate, and break down these polymers. Specifically, endo-glucanase 16 (EG16) enzymes, which are related to the well-known xyloglucan endotransglycosylase/hydrolase (XTH) gene products in Glycoside Hydrolase Family 16 (GH16), have been implicated in the degradation of the $\beta(1,4)$ -linked backbone of mixed-linkage $\beta(1,3); \beta(1,4)$ -glucans (MLG) and xyloglucans. EG16 members are single-copy genes found in most plant clades but are absent from many eudicots, including the model plant *Arabidopsis thaliana*. Until recently, EG16 members had only been characterized in vitro, establishing their substrate specificity, protein structure, and phylogenetic history, but their biological function was unknown. Here we used a hybrid polar, *Populus alba* \times *Populus grandidentata* (P39), as a model to examine EG16 expression, subcellular localization, and pheno- and chemotypes of EG16-downregulated P39 plants. *Populus* EG16 expression is strong in young tissues, but RNAi-mediated downregulation did not impact plant growth nor the fine structure of the hemicellulose xyloglucan, suggesting a restricted or currently unknown role in angiosperm physiology.

KEYWORDS

endo-glucanase 16, mixed-linkage glucan, *Physcomitrella*, plant cell wall, *Populus*, xyloglucan

This is an open access article under the terms of the [Creative Commons Attribution-NonCommercial-NoDerivs](https://creativecommons.org/licenses/by-nc-nd/4.0/) License, which permits use and distribution in any medium, provided the original work is properly cited, the use is non-commercial and no modifications or adaptations are made.

© 2023 The Authors. *Plant Direct* published by American Society of Plant Biologists and the Society for Experimental Biology and John Wiley & Sons Ltd.

1 | INTRODUCTION

Plant cells are enclosed by composite walls of partially crystalline cellulose, pectins, hemicelluloses, structural proteins, and, in secondary cell walls, lignin (Schultink et al., 2014). Hemicelluloses interact non-covalently with cellulose, and act as “spacers” between microfibrils (Braybrook & Jönsson, 2016; Cosgrove, 2022; Scheller & Ulvskov, 2010; Somerville et al., 2004). One of the hemicelluloses, xyloglucan, is a highly branched matrix glycan that makes up as much as 20% of the primary cell wall dry weight (Eklöf et al., 2012). Xyloglucan is the most common hemicellulose in the primary wall of angiosperms (Kozlova et al., 2020), with the exception of graminaceous monocots (Poales), where arabinoxylan and mixed-linkage β -glucan (MLG) are predominant (Kozlova et al., 2020; Popper et al., 2011).

Plant cell wall polysaccharides are produced, maintained, and modified by carbohydrate-active enzymes (CAZymes), which are abundant in plant genomes (Coutinho et al., 2003). Hence, CAZymes directly influence cell wall structure and function in plant growth and development, signaling, and defense (Pinard et al., 2015). A major group of plant CAZymes is encoded by the *xyloglucan endotransglycosylase/hydrolase (XTH)* gene family, members of which modify xyloglucan (EC 2.4.1.207 and EC 3.2.1.151) or perform *heterotransglycosylation* with other cell wall polysaccharides (Eklöf & Brumer, 2010; Ishida & Yokoyama, 2022; Stratilova et al., 2020). *XTH* gene products have thus been implicated in various physiological processes involving the cell wall, including morphogenesis of vegetative tissues and fruit ripening (Ishida & Yokoyama, 2022; Stratilova et al., 2020). These enzymes were previously the only known members of Glycoside Hydrolase Family 16 (GH16) in plants, comprising 20–60 homologs in individual species (Behar et al., 2018; Eklöf & Brumer, 2010; Michel et al., 2001; Viborg et al., 2019).

Recently, a unique group of CAZymes, designated endo-glucanase 16 (EG16), were identified as a sister clade to the *XTH* gene products in GH16 (Behar et al., 2018; Eklöf et al., 2013). EG16 members are distinguished structurally by a lack of the characteristic C-terminal extension found in all *XTH* gene products (PFAM XET_C, PF06955) (Eklöf et al., 2013; Eklöf & Brumer, 2010; McGregor et al., 2017). Also notable, EG16 members are found only as a single copy per plant genome and are highly conserved (ca. 70% sequence identity across very diverse species), yet have been lost from many taxa including many eudicots (Behar et al., 2018, 2021). For example, the absence of an EG16 ortholog in the model plant *Arabidopsis thaliana* has undoubtedly contributed to this group of enzymes being overlooked. On the other hand, extensive cross-genome surveys and phylogenetic analyses suggest a broad distribution of EG16 orthologs, including in the earliest plant lineages, for example, extant green algae (Jiao et al., 2020; Shinohara & Nishitani, 2021).

Biochemical characterization *in vitro* likewise suggests a divergent functional role of EG16 members *vis-à-vis* *XTH* gene products, the latter of which are predominantly xyloglucan endo-transglycosylases (Baumann et al., 2007; Kaewthai et al., 2013). EG16 members from poplar (*Populus trichocarpa*), grapevine (*Vitis vinifera*), and spreading earthmoss (*Physcomitrium [Physcomitrella] patens*) all exhibit broad hydrolytic activity toward MLG, xyloglucan, and soluble cellulose

derivatives (Behar et al., 2021; Eklöf et al., 2013; McGregor et al., 2017). The substrate specificities and product profiles of these orthologs are remarkably similar, despite circa 500 million years of evolutionary divergence (Behar et al., 2018).

Due to the recent identification of EG16 orthologs, their function *in vivo* is generally unknown. Recent analysis of the *P. patens* EG16 ortholog demonstrated high expression in young, developing tissues, and localization to the cell wall despite lacking a signal peptide. *PpEG16* gene-deletion plantlets were slightly larger than wild-type plants and exhibited earlier senescence (Behar et al., 2022). However, in the absence of an obvious strong phenotype in knock-out lines, the physiological role of these enzymes remains unclear. It is likewise unknown how EG16 function might be conserved across divergent taxa. Hence, in the present study we used the genetically tractable hybrid poplar *Populus alba* \times *Populus grandidentata* (P39) to extend our previous *in vitro* characterization of a *Populus* EG16 ortholog (Eklöf et al., 2013) to include *in planta* localization, and pheno- and chemotyping of EG16-downregulated P39 plants.

2 | MATERIALS AND METHODS

2.1 | Data sources

The *PtEG16* sequence was accessed from JGI Phytozome (accession number: POPTR_0002s15460) (Goodstein et al., 2012). Microarray and RNA-sequencing expression data were acquired from the eFP browser (Winter et al., 2007) and PopGenIE databases (Sjödin et al., 2009; Sundell et al., 2015), respectively (accession number: Potri.002G153200.1).

2.2 | Poplar growth conditions

Hybrid poplar *P. alba* \times *P. grandidentata* (P39) was grown in tissue culture using woody plant media (McCown & Lloyd, 1981) supplemented with .01- μ M 1-naphthaleneacetic acid and Plant Preservative Mixture (Plant Cell Technology) in Magenta vessels (GA-7; Millipore Sigma) under a 16-h light/8-h dark cycle with full-spectrum lighting at 24°C. Individual plants were cultured using aseptic techniques every 6 months.

2.3 | gDNA extraction

One hundred milligrams of leaf tissue was ground with a pestle in a 1.7-ml tube and subsequently mixed with 400- μ l DNA extraction buffer (200-mM Tris-HCl, 250-mM NaCl, 25-mM EDTA, .5% [w/v] SDS). The suspension was centrifuged for 3 min at 20,000 \times g, and the supernatant was then gently mixed with an equal volume of isopropanol and incubated for 10 min at ambient temperature. After centrifugation at 20,000 \times g for 5 min, the supernatant was discarded, and the pellet was washed with 70% ethanol, centrifuged again, and then the pellet was



air-dried in a sterile environment. Finally, the pellet was resuspended in 100- μ l sterile ddH₂O.

2.4 | Cloning

For cloning of the promoter–GUS construct, a 2000-bp sequence upstream of the translational start site of the *PtEG16* gene was amplified from *P. trichocarpa* Nisqually-1 gDNA by polymerase chain reaction (PCR) (Table S1). The product was inserted into pCR-Blunt II-TOPO and transformed into *Escherichia coli* using heat shock and then grown on LB plates containing 50 μ g/ml kanamycin for selection. The promoter fragment was transferred into Gateway donor vector pDONR221-Zeo using a BP reaction, and an LR reaction was then employed to transfer the promoter–GUS fragment into pMDC162 (Curtis & Grossniklaus, 2003). A plasmid preparation of the final construct was then used to transform *Agrobacterium tumefaciens* EHA105, as previously described (Wise et al., 2006).

For the RNAi (*EG16*-downregulated) lines (RC8), the *PtEG16* coding sequence was amplified from *P. trichocarpa* Nisqually-1 gDNA, inserted into pCR-Blunt II-TOPO and transformed into *E. coli*. A segment that does not share homology to other parts of the genome was amplified from the pCR-Blunt II-TOPO plasmid, cloned into pDONR221 using a BP reaction (Gateway Cloning, ThermoFisher Scientific), and then transformed into *E. coli*. An LR reaction was then used to transfer the RNAi fragment into pHELLSGATE12 (Helliwell & Waterhouse, 2003) and the resulting plasmid was transformed into *E. coli*. Finally, the purified plasmid was transformed into *A. tumefaciens* EHA105.

For the overexpression lines, the coding sequence of *EG16* and flanking regions were amplified from a cDNA preparation of *P. trichocarpa* Nisqually-1 by PCR. This fragment was cloned into pCR-Blunt II-TOPO and transformed into *E. coli*. The *PtEG16* coding sequence was then amplified by PCR, cloned into pDONR221-Zeo using a BP reaction, and then transformed into *E. coli*. The coding sequence was transferred into pMDC32 (Curtis & Grossniklaus, 2003) using an LR reaction. The resulting plasmid containing a 2X35S promoter and the *PtEG16* coding sequence was then transformed into *A. tumefaciens* GV3101.

2.5 | Plant transformation and genotyping

P39 poplar plants were transformed by *Agrobacterium*-mediated transformation of leaf discs, as described previously (Mottiar et al., 2022). For genotyping, gDNA was extracted from leaf tissue of each plant line as described above. PCR was carried out using 40 ng as a template (Standard Taq; NEB).

2.6 | RNA extraction, cDNA preparation, and RT-qPCR

RNA was extracted from leaf tissue as previously described (Kolossova et al., 2004), treated with DNase (DNA-free kit; Ambion), and cDNA

was prepared using the iScript cDNA Synthesis kit following manufacturer's instruction (Bio-Rad). Reverse transcriptase (RT)-quantitative PCR (qPCR) of the RNAi lines was completed using SsoAdvanced Universal SYBR Green (Bio-Rad). cDNA was made using primers targeting *PtEG16* and the 18S ribosomal RNA sequence as a reference (primer sequences are listed in Table S1). A two-step protocol was used on a CFX96 Touch Real-Time PCR Detection System.

2.7 | Tissue sectioning

Fresh tissue was sandwiched between two pieces of expanded polystyrene for physical support and sectioned transversally using a sliding microtome (American Optical 860 Sliding Microtome) to a thickness of 80–120 μ m.

2.8 | Promoter–GUS analysis

Six GUS-lines were grown in the greenhouse for three months, after which stems, petioles, and leaves were collected from young (first to fifth node) and mature (eighth node) nodes, and then sectioned. Sections were immersed in 90% cold acetone and incubated at 4°C for 20 min, after which they were washed with rinse solution (50 mM sodium phosphate buffer pH 7.2, 1-mM K₃Fe(CN)₆, .5-mM K₄Fe(CN)₆). Staining solution (.1-M sodium phosphate buffer pH 7.2, 10-mM EDTA, 1-mM K₃Fe(CN)₆, .5-mM K₄Fe(CN)₆, 1-mM X-Gluc) was applied next, and the tubes were vacuum-infiltrated three times for 1 min each in a desiccator after which the tissue was incubated for 1 h at 37°C to allow the β -glucuronidase to react with the substrate. For chlorophyll removal, sections were rinsed in ethanol solutions of increasing concentrations (15% to 100%), then gradually decreasing to 70% ethanol.

2.9 | Antibodies

Custom polyclonal antibodies targeting the full-length recombinant *PtEG16* were produced in *E. coli* by Cedarlane (Burlington, Ontario, Canada), as previously described (Eklöf et al., 2013). Additional anti-*PtEG16* polyclonal antibodies were raised against a polypeptide sequence, VEKREGGFPEKP, that is unique to *PtEG16*, conserved in other *Populus* species, and distinct from *P. trichocarpa* XTH gene products (Agrisera, Vännäs, Sweden).

2.10 | Western blotting

PtEG16 (Eklöf et al., 2013) was serially diluted (1–.0001 μ g) and boiled with Laemmli sample buffer (60-mM Tris-HCL, 1.5% (w/v) SDS, 8% (w/v) glycerol, .005% bromophenol blue, 100-mM dithiothreitol) for 15 min at 95°C. The samples were then loaded twice into different SDS-PAGE gels (Bio-Rad 4%–20% precast protein gels) alongside a protein ladder (BLUelf prestained protein ladder) and run at 180 V for

45 min. One gel was stained with Coomassie dye for 20 min, destained overnight, and then imaged (Bio-Rad ChemiDoc MP Imaging System). The other gel was transferred to a PVDF membrane (Millipore-Sigma) in a Bio-Rad Trans-Blot Semi-Dry Transfer Cell in Towbin transfer buffer (25-mM Tris, 192-mM glycine, 10% [v/v] methanol) sandwiched between two thick pieces of filter paper (1703958; Bio-Rad) at 25 V, .35 mA, 5 W for 50 min, and then left to dry overnight. Next, the membrane was activated with 100% methanol and incubated with blocking buffer (5% (w/v) skim milk powder in Tris-buffered saline, .1% Tween-20 (TBST)) for 1 h at ambient temperature with gentle agitation. The membrane was then incubated with primary antibody, diluted 1:1000 in TBST, for 1 h with continuous rocking at room temperature. The membrane was then washed with TBST for 10 min and then incubated with 1:10,000 diluted, horseradish peroxidase-conjugated secondary antibody (AS10 833; Agrisera) for 1 h with continuous rocking at room temperature. Next, the membrane was washed three times for 10 min each. Lastly, a chemiluminescent Western substrate kit (CCH345; Bio-Helix) was used following the manufacturer's instructions and the membrane was imaged (Bio-Rad ChemiDoc MP Imaging System).

2.11 | Immunofluorescence

The tissue fixation protocol was adapted from (Zachgo et al., 2000). Stem, petiole, and leaf samples isolated from the first and eighth nodes were sectioned as described above and incubated in fresh fixative solution (50-mM PIPES pH 7.5, 5-mM MgSO₄, 5mM EGTA pH 7.5, 4% (w/v) paraformaldehyde) for 1.5 h with gentle agitation and then washed twice with TBST (10-mM Tris pH 7, .25 M NaCl, .1% Tween-20). Fixed samples were cleared in ethanol solutions by gradually increasing concentrations for 10 min each with slight agitation (25%, 50%, and 100%), and then they were once more incubated with the solutions in reducing concentrations. TBST was then used to wash the samples for 10 min. In 1.7-ml tubes, the samples were incubated in blocking solution (5% bovine serum albumin in TBST) for 1 h at room temperature with gentle agitation. Subsequently, the blocking solution was discarded and incubated with primary antibody diluted in TBST (1:16 anti-PtEG16(full-length) antibodies, 1:20 anti-PtEG16(peptide) antibodies, 1:36 anti-homogalacturonan antibodies (JIM7, CarboSource, USA), 1:36 anti-xyloglucan (LM15, ab190146; Abcam), and 1:36 anti-(1,3;1,4)-β-glucan (anti-MLG) (BG1/BS 400-3, Biosupplies Australia)) for 2 h at room temperature. The samples were then washed twice with 200 μl TBST for 5 minutes and then incubated with secondary antibody (Alexa Fluor 488 anti-rat (A-11006), anti-mouse (A-11001), or anti-rabbit (A-11008) from Invitrogen) overnight at 4°C with gentle agitation. Finally, the samples were washed twice as described above.

2.12 | Microscopy

GUS samples were mounted in 70% glycerol on microscope slides (FroggaBio, Concord, Ontario, Canada), covered with coverslips, and

imaged with a Leica DMR microscope equipped with a Canon EOS Rebel T5 camera using Leica 10x/Air, 40x/Air, and 64x/Oil lenses. Immunostained samples were mounted on microscope slides in TBST and covered with coverslips. The samples were imaged on an Olympus FV1000 Laser Scanning microscope using 10x/NA .4/Air, 40x/NA .95/Air, and 60x/NA 1.1 WD 1.5-mm lenses using the default settings for Alexa Fluor 488.

2.13 | Growth assay

Wild-type P39 and several RNAi lines (RC8-4, RC8-6, RC8-8, RC8-10, RC8-14, and RC8-16) were grown for 5 weeks in tissue culture and then potted in perennial soil (50% peat, 25% humus, and 25% crushed bark chips) in 2-gal pots in a greenhouse. The photoperiod length was 16 h, and the LED light output was ~250 μmol/m²/s at the table surface. After 4.5 months of growth, the following parameters were measured: plant height, number of leaves, third petiole and eighth petiole diameter at the base, third and eighth petiole total length, third to fourth and eighth to ninth internode stem diameter (below top petiole), and third to fourth and eighth to ninth internode stem length. Data were analyzed using a one-way analysis of variance (ANOVA) with post hoc Student's *t*-tests and a Bonferroni–Holm correction.

2.14 | Soluble sugar analysis

Soluble sugars were quantified in the leaves of 3-month-old RNAi and wild-type plants. To determine a difference between the higher and lower expressing tissues of *EG16*, the first to fifth leaves (designated as “young”) and the eighth leaf (designated as “mature”) were collected from greenhouse-grown plants and frozen in liquid nitrogen. The analysis followed a previously described protocol (Da Ros et al., 2020). The data were analyzed using a one-way ANOVA with post hoc Student's *t*-tests and a Bonferroni–Holm correction.

2.15 | Mass spectrometry analysis of wall polysaccharides

For the imaging of hemicellulose in the tissue sections, plant specimens (third to fourth internode stems) were fixed in 4% formaldehyde in 1X PBS. Samples were vacuum-dried and stored at 4°C. After fixation, the samples were embedded in 10% low-melt agarose (Sigma Aldrich). Agarose blocks were incubated at 4°C overnight and covered with wet tissue paper to prevent dehydration during hardening. Agarose-embedded specimens were then cut into 80-μm-thick sections using a vibratome (Leica VT 1000S).

For regular mass spectrometry analysis of hemicelluloses, oligosaccharide mass profiling was carried out as previously described (Obel et al., 2009). In brief, tissue material was subjected to an alcohol-insoluble residue preparation to eliminate possible protein



or lipid contamination. This preparation comprises three main incubation steps, 2 min each: 70% aqueous ethanol; 1:1 (v/v) methanol/chloroform; and absolute ethanol. After each step, the eluent was removed and the sample was air-dried for 1 min. The alcohol-insoluble material was then stored in 70% ethanol at room temperature, or stored at 4°C for later use. Xyloglucan and MLG present in the alcohol-insoluble residue were enzymatically digested utilizing an endo- β -1,4-glucanase (XEG) (Pauly et al., 1999) and a lichenase (*E-LICHN*; Megazyme), respectively, in independent experiments. Released oligosaccharides were then analyzed by matrix-assisted laser desorption ionization-time of flight (MALDI-TOF) mass spectrometry. The matrix chemical used for the MALDI-TOF analysis was 100 mg/ml of 2,5-dihydroxybenzoic acid (DHB) dissolved in a mixture of 1:1 H₂O/acetonitrile (Carl-Roth) containing 2% of N,N-dimethylaniline (DMA, Fisher Scientific) (Snovida et al., 2008) and 15-mM NaCl. The matrix was sprayed onto the (digested) samples using the HTX TM-sprayer at 25°C, at a flow rate of .1 ml/min. As controls, 1 μ l of β -1,3-cellobiose (10 mg/ml, Megazyme) was spotted onto the slide with MLG-digested samples and 1 μ l of a mixture of tamarind xyloglucan oligosaccharides (1 mg/ml, Megazyme) was spotted onto the slide with the xyloglucan digested samples. Both solutions were spotted prior to matrix deposition and vacuum dried.

Indium-tin-oxide (ITO) coated slides (Bruker, Bremen, Germany) for mass spectrometry imaging were poly-L-lysinated (poly-L-lysine [PLL] solution; P8920; Sigma). Sections were placed on these PLL-ITO-coated slides. Images of sections were acquired with a bright-field microscope (Leica Application Suite, Leica camera DFC 420C). The images of sections were stitched together and scaled using ImageJ software (Preibisch et al., 2009; Schindelin et al., 2012).

For release of hemicellulose oligosaccharides, enzyme solutions were sprayed with an HTX TM-sprayer (Bruker Daltonic) at 30°C on sections placed on the PLL-ITO-coated slides. Xyloglucan was enzymatically digested with 50 μ g/ μ L XEG (Pauly et al., 1999) in 25 mM ammonium formate buffer, pH 4.5. MLG was treated with 50 μ g/ μ L of lichenase (Megazyme), resuspended in 50 mM ammonium acetate, pH 6.5. Both enzyme solutions were sprayed at a flow rate of 7.5 μ l/min. As a positive control to verify enzyme digestion, *A. thaliana* alcohol insoluble residue and barley alcohol insoluble residue were spotted on the slides and vacuum dried. After spraying the enzyme, the slides treated with XEG were incubated for 20 min at 37°C and the slides treated with lichenase were incubated for 1 h at 50°C for enzymatic digestion.

Data collection was performed with a Rapiflex Tissue typer MALDI-TOF mass spectrometer controlled with FlexControl 4.0 (Bruker, Bremen, Germany) in positive reflector mode collecting 2000 hits per laser shot. An optical image of the slide was obtained using the FlexImaging 5.0 (Bruker, Bremen, Germany) software for selected areas. The raster width for obtaining the images was set to 25x25 μ m. The images were processed using FlexImaging 5.0. The resulting spectra were normalized according to the root-mean-square (RMS) of the data points (Deining et al., 2011).

3 | RESULTS

3.1 | *Populus* EG16 localizes to young and expanding tissues

The eFP browser (Winter et al., 2007) and PopGenIE (Sjödin et al., 2009; Sundell et al., 2015) databases were queried to determine the expression levels of *PtEG16* in *P. trichocarpa* tissues (Figure S1). Expression was highest in male and female catkins (584 \pm 108 RMA and 517 \pm 123 RMA, respectively, Figure S1a). Young leaves and roots had two-fold lower expression, while seedlings and mature leaves exhibited the lowest expression levels, ca. four-fold and ten-fold lower than in young leaves, respectively (Figure S1a). In accordance with the microarray data, quantitative RNA-sequencing demonstrated that the maximum expression occurred in developing catkins and field-grown expanding leaf buds, whereas the lowest expression was found in mature leaves (Figure S1b).

To discern expression differences between various tissue types and cells, hybrid poplar P39 was transformed with a *PtEG16* promoter:: β -glucuronidase (*pPtEG16::GUS*) construct; successful transformation was established via genotyping (Figure S2a). Based on the microarray and RNA-sequencing analyses, the promoter-GUS analysis focused on contrasting juvenile and mature tissues (Figure 1). GUS staining of young (first to fifth node) and mature (eighth node) leaves, petioles, and stems showed that expression is strong in the epidermis, cortical parenchymal cells, and in the pith of young petioles and stems, and is almost non-existent in mature tissues (Figure 1). Young leaves showed higher expression in the apical side of the blade, in the epidermis and in the cortex, and lower expression in the epidermis of the leaf vein. No staining was observed in the cortex, pith, and vascular tissues of the vein. GUS-stained young stems and petioles presented a pattern in which staining was pronounced in cells surrounding sclerenchyma in the cortex (Figure 1).

As *EG16* genes do not encode signal peptides (Behar et al., 2018), cytosolic localization would normally be predicted. This is incongruent with the localization of the known substrates of *PtEG16* and other *EG16* members (β -glucans, including MLG and xyloglucan), which are generally present in the apoplast, and in the Golgi apparatus, the location of their synthesis (Eklöf et al., 2013). Hence, polyclonal antibodies were generated against the full-length, recombinant *PtEG16* protein for localization studies (Figure S3). Immunolocalization using this antibody preparation showed binding to the cell walls of all tissues examined (Figure S4). In particular, the strong fluorescence from mature petioles contradicts *EG16* expression analyses that showed low expression in older tissues (Figure 1). Additional tests using petioles of tomato (*Solanum lycopersicum*), which does not have an *EG16* homolog (Behar et al., 2018), suggested that this antibody suffers from non-specific binding, perhaps to sequence-related *XTH* gene products (Figure S4).

To resolve this problem, additional polyclonal antibodies were generated against a short, synthetic peptide from *PtEG16* (VEKREGEGFPEKP) that is not present in *PtXTH* orthologs or other proteins in the *P. trichocarpa* proteome (Figures S5 and S3). Subsequently, immunofluorescence experiments on petiole cross-sections

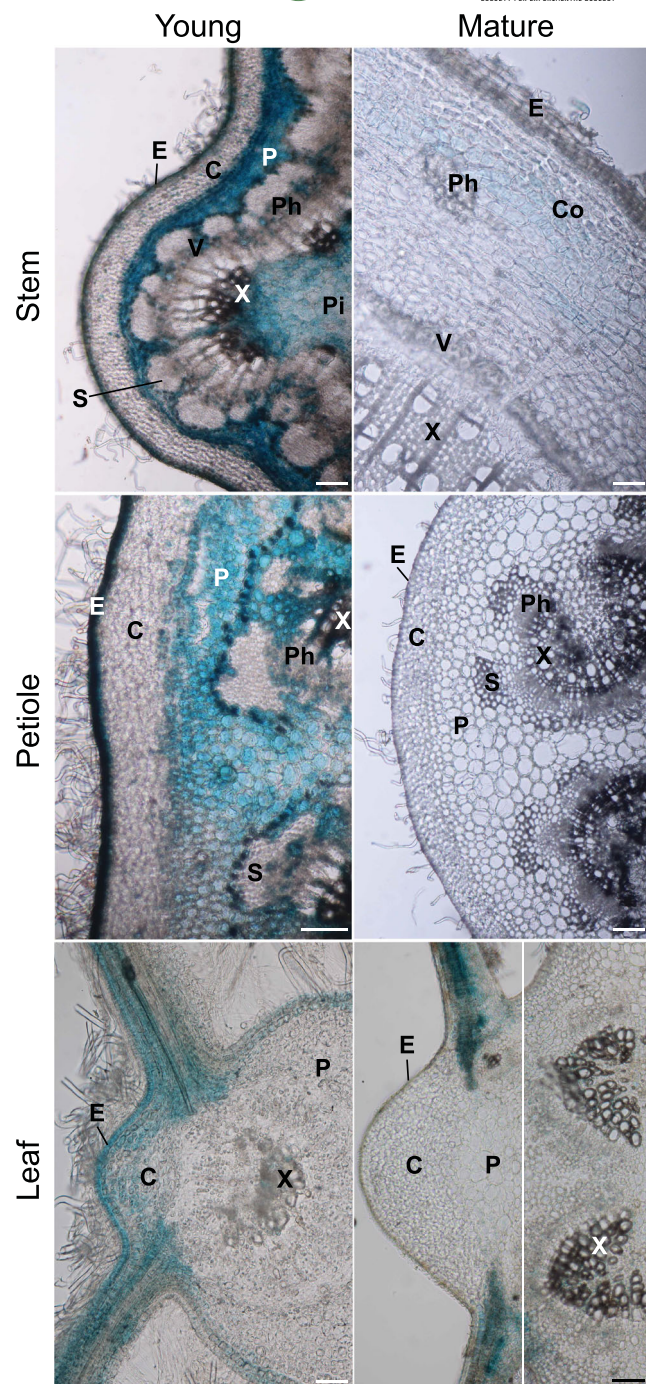


FIGURE 1 Promoter- β -glucuronidase assays of transverse sections of P39 poplar lines expressing *pPtEG16::GUS*. Scale bars represent 100 μ m. C, cortical collenchyma cells; Co, cortex; E, epidermis; P, cortical parenchyma cells; Ph, phloem; Pi, pith; S, sclerenchyma; V, vascular cambium; X, xylem

showed a stronger signal in young tissues (Figure 2a) that was not present in controls lacking primary antibody. Binding was observed in young petiole sections in the walls of the cortex and, to a lesser extent, in the cell walls of vascular tissue. A signal also appears in the cortical collenchyma cells of young petioles, where the promoter::

GUS studies indicated a low *EG16* expression (Figure 2a). In mature tissues, the signal appeared not in the apoplast but only as large intracellular puncta (Figure 2a). Generally, these observations indicate specific and strong binding in tissues where *EG16* is expressed, and weak or no binding in mature tissues.

3.2 | *Populus EG16* downregulation does not affect plant morphology

PtEG16 expression was downregulated in P39 hybrid poplar by RNAi. Of the 20 lines selected, 15 contained the RNAi construct, as verified by PCR (Figure S2b). RT-qPCR analysis showed that expression was downregulated by 60%–90% in all lines except for lines 11 and 13 (Figure S6). The lines RC8-4, RC8-6, RC8-8, RC8-10, RC8-14, and RC8-16 were subsequently selected for further study and grown in the greenhouse for 4.5 months.

Using the peptide-based polyclonal antibodies, a signal was still observed in young tissues, but to a lower extent than in wild-type tissues (Figure 2b), thereby indicating that downregulation of *EG16* was successful in reducing protein abundance. In addition, faint binding to vascular cell walls was observed, although this may be due to autofluorescence.

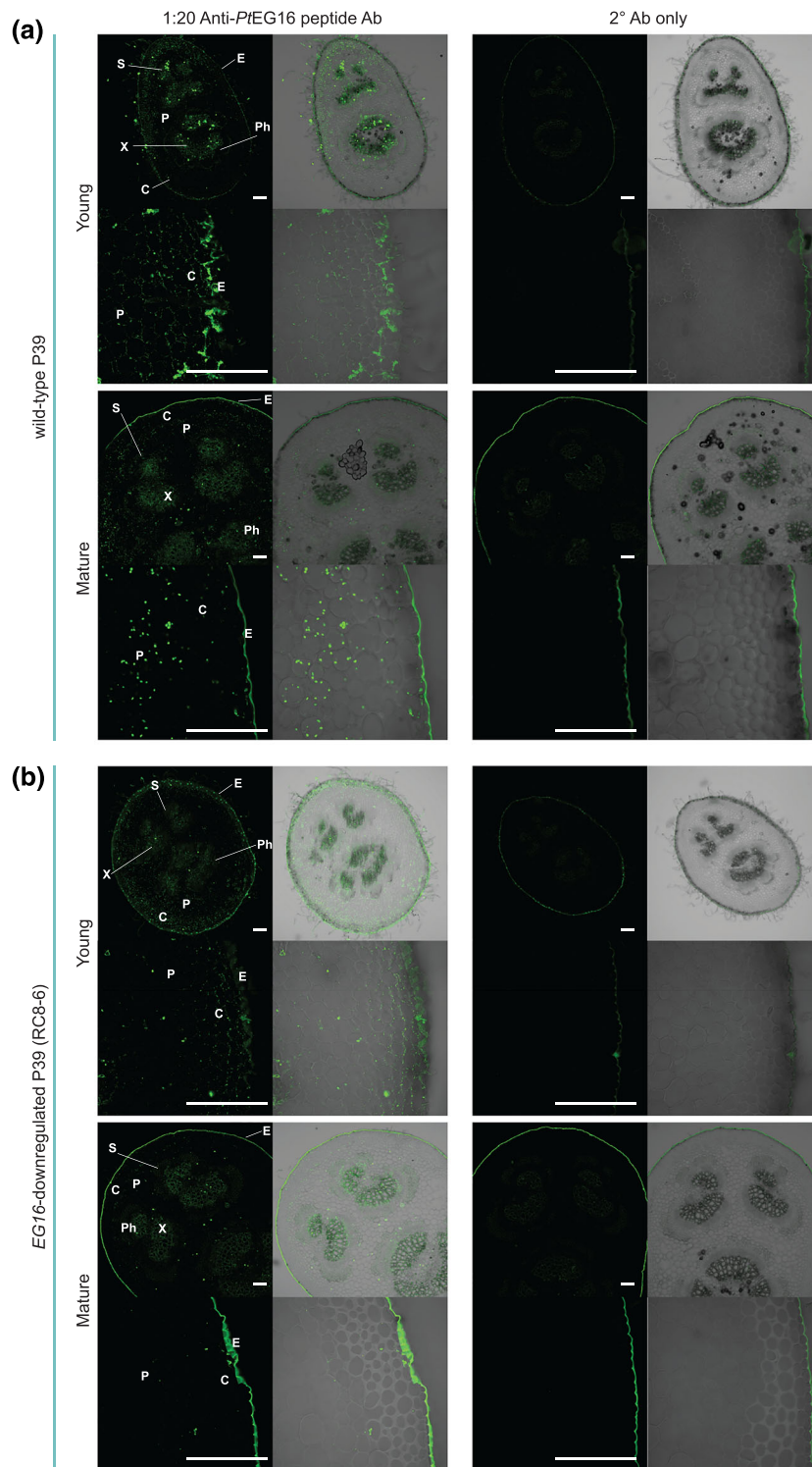
Morphological differences were not observed between the wild-type and RNAi plants, including plant height, number of leaves, young and mature petiole diameter and length, and young and mature internode stem diameter and length (Figure 3). An exception was line RC8-4, which displayed significantly larger young and mature petiole diameters (119% and 121% compared to wild-type, respectively), and longer mature petioles (122% longer than wild-type, Figure 3). Line RC8-4 was the downregulated line with the lowest expression of *EG16* (Figure S6). However, the expression level in line RC8-10 was comparable, yet significant growth phenotypes were not observed in this line. The observation that only one of the six lines showed significant growth phenotypes in comparison to the wild-type precludes any definitive conclusion on the effect of *EG16* downregulation on plant development under the conditions examined.

3.3 | *Populus EG16* downregulation does not affect carbohydrate levels

To determine if the downregulation of *PtEG16* affects its known substrates (Eklöf et al., 2013), the presence of MLG and xyloglucan was analyzed *in situ*. Although xyloglucan is a known component of *Populus* cell walls, MLG has not been identified in poplar tissues thus far (Popper et al., 2011). Immunolocalization and oligosaccharide mass profiling were performed to determine the presence and distribution of both polysaccharides in tissues expressing *EG16*.

Immunolocalization of MLG in young and mature petioles of wild-type and *EG16*-downregulated plants with anti-MLG antibodies resulted in the appearance of dim puncta covering various areas of

FIGURE 2 Confocal microscopy of immunolabelled wild-type P39 (a) and *EG16*-downregulated poplar (RC8-6) (b) sections using anti-PtEG16 peptide antibodies. Sectioned petiole tissue from greenhouse-grown plants. Young = 2nd node petiole, mature = 8th node. Scale bars represent 100 μm . C, cortical collenchyma cells; E, epidermis; P, cortical parenchyma cells; Ph, phloem; S, sclerenchyma; X, xylem



the tissue (Figure S7a). In contrast, immunolocalization of MLG in maize roots, where it is a predominant component of the grass cell wall, results in strong, continuous fluorescence throughout the wall (Kozlova et al., 2020). Thus, the observed labeling pattern in these poplar tissues is likely to be nonspecific binding. Concomitantly, mass spectrometry analysis of alcohol insoluble residues treated with a specific mixed-linkage endoglucanase failed to evidence the expected tri- and tetrasaccharides (m/z 527 and 689, respectively) in both wild-type

and *EG16*-downregulated plants (Figure S7b). Thus, no MLG was detected in poplar tissues using two complimentary methods, which is consistent with current knowledge of cell wall composition across plant taxa (Popper et al., 2011).

Xyloglucan is also a substrate of PtEG16 in vitro (Eklöf et al., 2013) and is a prominent component of poplar cell walls (Bourquin et al., 2002; Gerttula et al., 2015; Mellerowicz et al., 2008). To determine whether there may be differences in xyloglucan

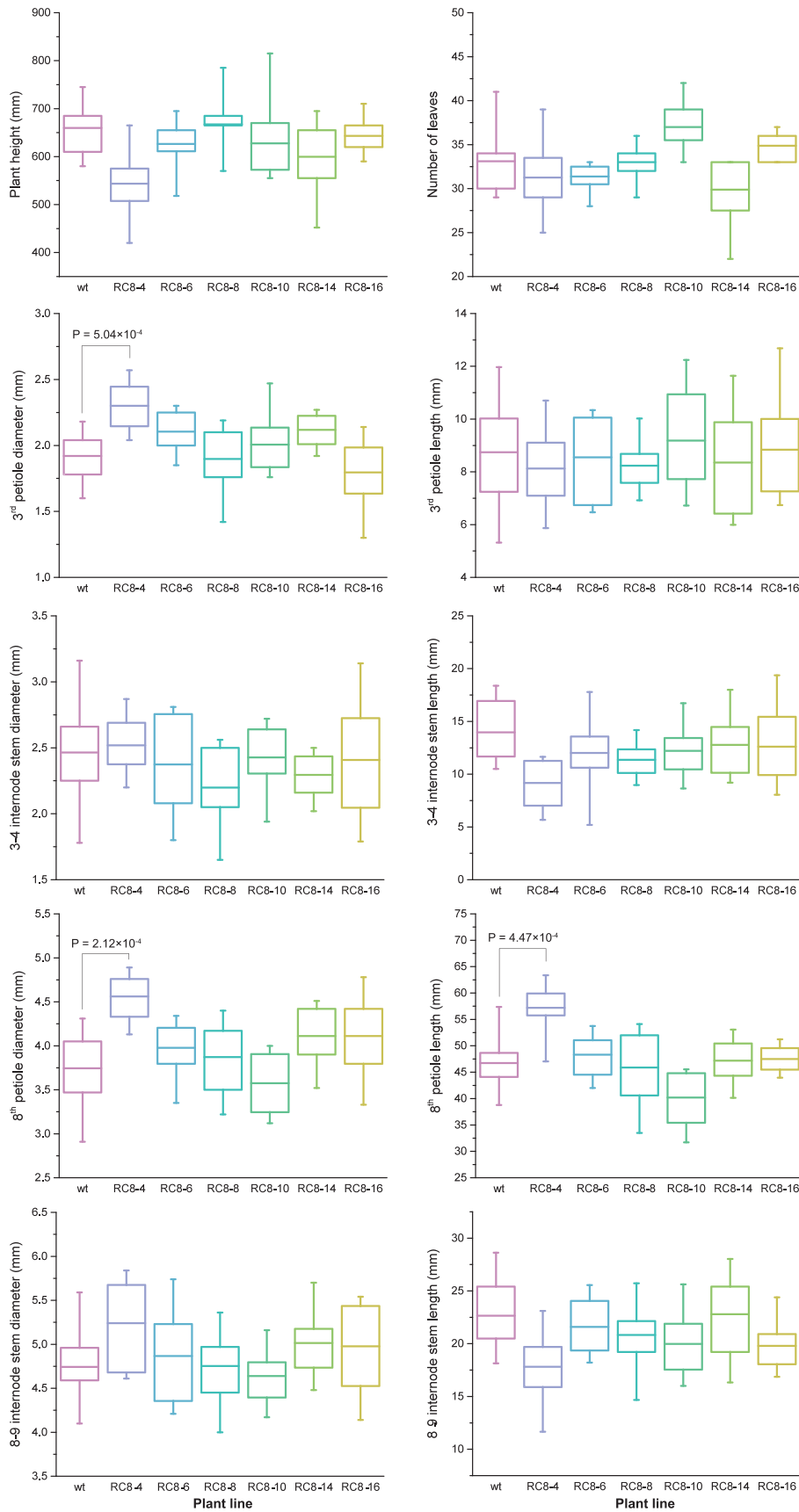


FIGURE 3 Phenotyping of *EG16*-downregulated lines. Growth parameters of each line ($N = 8$) were measured after 4.5 months of growth. Boxplots represent measurements from 25th to 75th percentiles, and whiskers denote the minimum and maximum measurements. Statistical significance (P) was calculated following one-way ANOVA and post hoc Student's t -tests with Bonferroni-Holm correction.

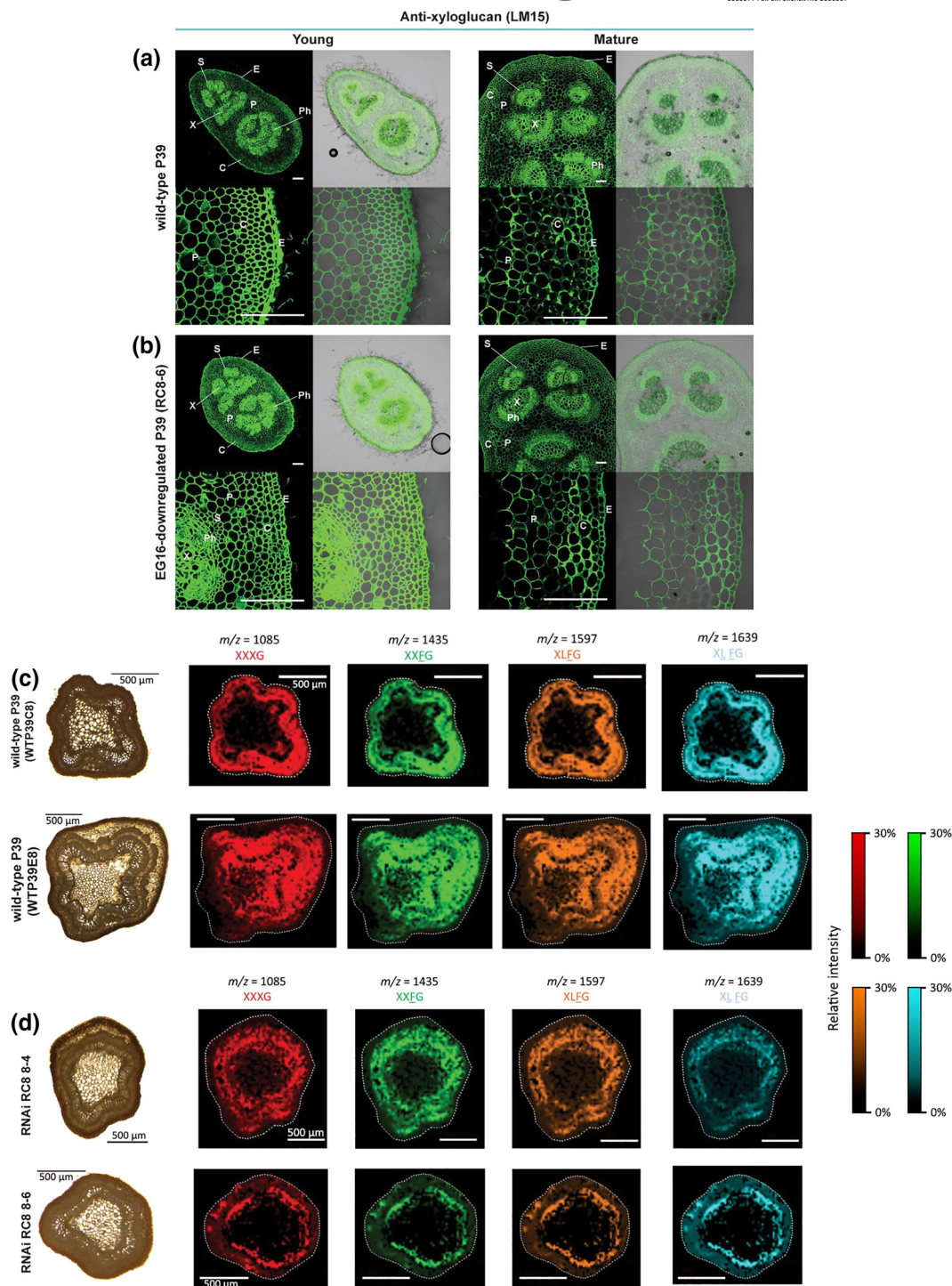


FIGURE 4 Analysis of *PtEG16* substrate xyloglucan in P39 tissues. Confocal microscopy of immunolabelled P39 poplar (a) and *EG16*-downregulated P39 (b) using anti-xyloglucan antibodies (LM15). Scale bars in (a) and (b) represent 100 μm . C, cortical collenchyma cells; E, epidermis; P, cortical parenchyma cells; Ph, phloem; S, sclerenchyma; X, xylem. MALDI-imaging of xyloglucan ions in the tissues of wild-type P39 (c) and in two *EG16*-downregulated lines (d). Sections of third to fourth internode stems were treated with a xyloglucanase and inserted into a MALDI-TOF mass spectrometer. Scale bars in (c) and (d) represent 500 μm ; dotted lines delineate regions of interest. False-color images of selected ions were assembled from the mass spectra obtained from each 25- μm raster width and are plotted according to relative ion intensity, which were normalized according to the root-mean-square (RMS) of the data points (Deininger et al., 2011).

composition between wild-type and *EG16*-downregulated plants, tissue sections were treated with anti-xyloglucan antibodies in wild-type and *EG16*-downregulated petioles. As expected, the cell walls of all

tissues tested displayed extensive labeling; however, no obvious differences between plant lines were observed (Figure 4a,b). Mass spectrometry imaging utilizing a xyloglucan endo- β -1,4-glucanase

(Veličković et al., 2014) was also performed to assess differences in xyloglucan fine structure in epidermis, phloem, and collenchyma tissues of young stems. The expected eudicot (fuco)galactoxyloglucan oligosaccharides were observed in all samples at similar ratios (Figure S8). Images of stem sections showed that the pith lacked detectable xyloglucan, likely due to the presence of large cells and hence low wall density in this tissue (Figure 4c,d). Consistent with the immunostaining results, xyloglucan was observed by mass spectrometry imaging in various tissue regions, and its distribution did not differ between the plant lines and the tissues tested (Figures 4a,b and 4c,d).

To probe potential metabolic differences between the wild-type and *PtEG16* RNAi lines, the soluble sugars galactose, sucrose, myoinositol, fructose, raffinose, and glucose were quantified in young and mature leaf tissue. RNAi lines RC8-8 and RC8-16 tissues had significantly lower glucose levels compared to wild-type, both in young and mature tissues. However, these differences were not consistent across all the downregulated lines (Figure S9).

4 | DISCUSSION

The biochemical and phylogenetic characterization of *PtEG16* was the first to distinguish *EG16* gene products as a distinct clade of plant GH16 enzymes vis-à-vis the well-known *XTH* gene products (Eklöf et al., 2013). Since then, an extensive bioinformatic analysis discerned the broad distribution of *EG16* orthologs in the plant kingdom (Behar et al., 2018). *EG16* members are highly conserved across the plant kingdom as single-copy genes (Behar et al., 2018), and this conservation extends to substrate specificity and protein structure (Behar et al., 2021; Eklöf et al., 2013; McGregor et al., 2017).

In the present study, promoter-GUS assays in P39 hybrid poplar showed that *EG16* expression is high in young tissues, specifically in cortical parenchyma cells, with no expression apparent in cortical collenchyma cells and vascular bundles (Figure 1). This distribution is reminiscent of the moss *P. patens* *EG16* (Behar et al., 2022; Yokoyama et al., 2010), the monocot *Hordeum vulgare* (barley) (Akdemir et al., 2022), and the conifer *Picea abies* (Norway spruce) (Behar et al., 2018), in which *EG16* expression is associated with young and rapidly growing cell types. These data suggest a conserved role in early tissue development. In general, localization of the *Populus* *EG16* protein was observed in cells where the gene was lowly expressed, as indicated by promoter-GUS analysis. Localization using peptide-specific antibodies showed that the epitope was present in both cortical collenchyma and parenchyma cell walls in young tissues (Figure 2), despite their divergent *EG16* expression levels. However, these contrasting datasets are likely not due to nonspecific antibody binding because protein levels were clearly reduced in mature and *EG16*-downregulated tissues, where *EG16* expression is minimal (Figures 1 and S2). The inconsistency between localization studies could be an indication that the highly sensitive immunofluorescence assay may sufficiently detect the protein even at low expression levels. It is also possible that the use of the 2 kb promoter in the promoter-GUS analysis is missing cis-regulatory elements required to fully recapitulate wild-type expression.

As *EG16* genes do not encode signal peptides, it was essential to determine cellular localization to understand fully *Populus* *EG16* function in vivo. Observations from immunolocalization experiments showed that *EG16* localizes to cell walls (Figure 2). This result is consistent with previous studies of *EG16* in *P. patens* protonema tissues, which showed localization to the wall at cell tips (Behar et al., 2022). It is notable that the apparent signal-sequence-independent localization to the cell wall is conserved across the poplar and moss orthologs, which further supports the possibility of non-canonical protein secretion (discussed in Behar et al., 2022; see also Agrawal et al., 2010; Davis et al., 2016; De Caroli et al., 2021; Ruiz-May & Rose, 2013).

Numerous metrics showed no differences between wild-type and transgenic hybrid poplar lines in which *EG16* had been downregulated by RNAi. The parameters assessed included overall growth phenotypes (Figure 3), soluble sugar content (Figure S9), xyloglucan tissue localization (Figure 4a,b), and xyloglucan fine structure (Figure 4c,d, Figure S8). Noting that the transgenic lines still express *EG16* at low levels, it is possible that sufficient enzyme activity is generated to fulfill its biological role. Alternatively, the reduction of *EG16* activity may be compensated by unknown enzymes and wall mechanical rearrangements, or may only have a critical effect under specific environmental conditions. Similarly, genetic deletion of a pair of xyloglucan endohydrolase paralogs in *A. thaliana* did not affect plant growth and development (Kaewthai et al., 2013). In direct comparison, deletion of *EG16* in the bryophyte *P. patens* produced slightly larger plant colonies and resulted in earlier senescence (Behar et al., 2022). *EG16* homologs are more common in non-angiosperm plants and have been lost from many extant angiosperm genomes (Behar et al., 2018), suggesting that their function may be more dispensable in “higher” plants. The very high sequence conservation in eudicots compared to other lineages nonetheless still presents a conundrum (Behar et al., 2018). The role of *EG16* in *Populus* may be most important in catkins, the tissue that has the highest *EG16* expression (Figure S2). However, the extended time (years) required for *Populus* to achieve flowering maturity makes testing this hypothesis practically challenging.

In conclusion, this study represents the first attempt to characterize the function of an angiosperm *EG16* member in vivo using hybrid poplar as a model species. However, downregulation of the single *EG16* ortholog did not affect overall growth and morphology, nor hemicellulose architecture in cell walls. Thus, the broad and high conservation of *EG16* orthologs across vastly distant plant lineages remains enigmatic. Further work is therefore required, perhaps in combination with other mutations or environmental stresses, to elucidate the biological function(s) of these enzymes in diverse taxa. Certainly, the potential functions of *EG16* members should be considered alongside other plant beta-glucanases in developing a holistic view of cell wall development (Perrot et al., 2022).

ACKNOWLEDGMENTS

The authors thank UBC Greenhouse staff, Melina Biron and Taylor Scriber, and UBC Bioimaging Facility (RRID: SCR_021304), Dr. Miki Fujita, Kevin Hodgson, and Dr. Eunyoung Lee. The authors also acknowledge Dr. Faride Unda for her guidance on HPLC work and



poplar growth, Dr. Eliana Gonzales-Vigil for assistance with RT-qPCR analysis, and Michelle von Loessl (Mansfield Lab, UBC) for assistance with sectioning and GUS analysis. H. Behar thanks Dr. Letitia da Ros (Mansfield Lab, UBC), Dr. Sam Livingston (Samuels Lab, UBC), Micheal Bilek (Mansfield Lab, UBC) and Dr. Miranda Meents (Samuels Lab, UBC) for useful discussions.

CONFLICT OF INTEREST

The authors claim no conflict of interest.

AUTHOR CONTRIBUTIONS

H. Behar carried out the genotyping, GUS staining, RT-qPCR, growth assays, and immunofluorescence microscopy and made the related figures. Y. Mottiar and R. Chandrasehkar performed the gene cloning and poplar transformations. A. C. Grappadelli performed MALDI-imaging and made the associated figures. H. Brumer, S. D. Mansfield, M. Pauly, and A. L. Samuels provided guidance on experimental design and supervised the research. H. Behar, M. Pauly, and H. Brumer co-wrote the manuscript with input from the other authors.

DATA AVAILABILITY STATEMENT

All data generated from this study are included within this manuscript and supporting information.

ORCID

Yaseen Mottiar  <https://orcid.org/0000-0002-4106-6159>

Allegra Corelli Grappadelli  <https://orcid.org/0000-0003-4337-2042>

Markus Pauly  <https://orcid.org/0000-0002-3116-2198>

A. Lacey Samuels  <https://orcid.org/0000-0002-0606-8933>

Harry Brumer  <https://orcid.org/0000-0002-0101-862X>

REFERENCES

- Agrawal, G. K., Jwa, N. S., Lebrun, M. H., Job, D., & Rakwal, R. (2010). Plant secretome: Unlocking secrets of the secreted proteins. *Proteomics*, 10, 799–827. <https://doi.org/10.1002/pmic.200900514>
- Akdemir, H., Seven, M., Derman, U. C., & Harvey, A. J. (2022). In silico analysis of XTH gene family from barley (*Hordeum vulgare* L.) and their comparative expression analysis during germination. *Turkish Journal of Botany*, 46, 92–108. <https://doi.org/10.55730/1300-008X.2674>
- Baumann, M. J., Eklöf, J. M., Michel, G., Kallas, A. M., Teeri, T. T., Czjzek, M., & Brumer, H. (2007). Structural evidence for the evolution of xyloglucanase activity from xyloglucan endo-transglycosylases: biological implications for cell wall metabolism. *Plant Cell*, 19, 1947–1963. <https://doi.org/10.1105/tpc.107.051391>
- Behar, H., Graham, S. W., & Brumer, H. (2018). Comprehensive cross-genome survey and phylogeny of glycoside hydrolase family 16 members reveals the evolutionary origin of EG16 and XTH proteins in plant lineages. *Plant Journal*, 95, 1114–1128. <https://doi.org/10.1111/tbj.14004>
- Behar, H., Samuels, A. L., & Brumer, H. (2022). *Physcomitrium* (*Physcomitrella*) *patens* endo-glucanase 16 is involved in the cell wall development of young tissue. *Physiologia Plantarum*, 174, e13683. <https://doi.org/10.1111/ppi.13683>
- Behar, H., Tamura, K., Wagner, E. R., Cosgrove, D. J., & Brumer, H. (2021). Conservation of endo-glucanase 16 (EG16) activity across highly divergent plant lineages. *Biochemical Journal*, 478, 3063–3078. <https://doi.org/10.1042/BCJ20210341>
- Bourquin, V., Nishikubo, N., Abe, H., Brumer, H., Denman, S., Eklund, M., Christiernin, M., Teeri, T. T., Sundberg, B., & Mellerowicz, E. J. (2002). Xyloglucan endotransglycosylases have a function during the formation of secondary cell walls of vascular tissues. *Plant Cell*, 14, 3073–3088. <https://doi.org/10.1105/tpc.007773>
- Braybrook, S. A., & Jönsson, H. (2016). Shifting foundations: the mechanical cell wall and development. *Current Opinion in Plant Biology*, 29, 115–120. <https://doi.org/10.1016/j.pbi.2015.12.009>
- Cosgrove, D. J. (2022). Building an extensible cell wall. *Plant Physiology*, 189, 1246–1277. <https://doi.org/10.1093/plphys/kiac184>
- Coutinho, P. M., Stam, M., Blanc, E., & Henrissat, B. (2003). Why are there so many carbohydrate-active enzyme-related genes in plants? *Trends in Plant Science*, 8, 563–565. <https://doi.org/10.1016/j.tplants.2003.10.002>
- Curtis, M. D., & Grossniklaus, U. (2003). A gateway cloning vector set for high-throughput functional analysis of genes in planta. *Plant Physiology*, 133, 462–469. <https://doi.org/10.1104/pp.103.027979>
- Da Ros, L., Unda, F., & Mansfield, S. D. (2020). Determination of soluble carbohydrates. In F. Bärlocher, M. Gessner, & M. Graça (Eds.). *Methods to Study Litter Decomposition* (pp. 131–137). Springer. https://doi.org/10.1007/978-3-030-30515-4_15
- Davis, D. J., Kang, B. H., Heringer, A. S., Wilkop, T. E., & Drakakaki, G. (2016). Unconventional Protein Secretion in Plants. *Methods in Molecular Biology*, 1459, 47–63. https://doi.org/10.1007/978-1-4939-3804-9_3
- De Caroli, M., Manno, E., Piro, G., & Lenucci, M. S. (2021). Ride to cell wall: Arabidopsis XTH11, XTH29 and XTH33 exhibit different secretion pathways and responses to heat and drought stress. *The Plant Journal*, 107, 448–466. <https://doi.org/10.1111/tbj.15301>
- Deininger, S. O., Cornett, D. S., Paape, R., Becker, M., Pineau, C., Rauser, S., Walch, A., & Wolski, E. (2011). Normalization in MALDI-TOF imaging datasets of proteins: practical considerations. *Analytical and Bioanalytical Chemistry*, 401, 167–181. <https://doi.org/10.1007/s00216-011-4929-z>
- Eklöf, J. M., & Brumer, H. (2010). The XTH gene family: an update on enzyme structure, function, and phylogeny in xyloglucan remodeling. *Plant Physiology*, 153, 456–466. <https://doi.org/10.1104/pp.110.156844>
- Eklöf, J. M., Ruda, M. C., & Brumer, H. (2012). Distinguishing xyloglucanase activity in endo- β (1–4) glucanases. *Methods in Enzymology*, 510, 97–120. <https://doi.org/10.1016/B978-0-12-415931-0.00006-9>
- Eklöf, J. M., Shojania, S., Okon, M., McIntosh, L. P., & Brumer, H. (2013). Structure-function analysis of a broad specificity *Populus trichocarpa* endo- β -glucanase reveals an evolutionary link between bacterial licheninases and plant XTH gene products. *Journal of Biological Chemistry*, 288, 15786–15799. <https://doi.org/10.1074/jbc.M113.462887>
- Gerttula, S., Zinkgraf, M., Muday, G. K., Lewis, D. R., Ibatullin, F. M., Brumer, H., Hart, F., Mansfield, S. D., Filkov, V., & Groover, A. (2015). Transcriptional and Hormonal Regulation of Gravitropism of Woody Stems in *Populus*. *Plant Cell*, 27, 2800–2813. <https://doi.org/10.1105/tpc.15.00531>
- Goodstein, D. M., Shu, S. Q., Howson, R., Neupane, R., Hayes, R. D., Fazo, J., Mitros, T., Dirks, W., Hellsten, U., Putnam, N., & Rokhsar, D. S. (2012). Phytozome: A comparative platform for green plant genomics. *Nucleic Acids Research*, 40, D1178–D1186. <https://doi.org/10.1093/nar/gkr944>
- Helliwell, C., & Waterhouse, P. (2003). Constructs and methods for high-throughput gene silencing in plants. *Methods*, 30, 289–295. [https://doi.org/10.1016/S1046-2023\(03\)00036-7](https://doi.org/10.1016/S1046-2023(03)00036-7)

- Ishida, K., & Yokoyama, R. (2022). Reconsidering the function of the xyloglucan endotransglucosylase/hydrolase family. *Journal of Plant Research*, 135, 145–156. <https://doi.org/10.1007/s10265-021-01361-w>
- Jiao, C., Sørensen, I., Sun, X., Sun, H., Behar, H., Alseekh, S., Philippe, G., Palacio Lopez, K., Sun, L., Reed, R., Jeon, S., Kiyonami, R., Zhang, S., Fernie, A. R., Brumer, H., Domozych, D. S., Fei, Z., & Rose, J. K. C. (2020). The *Penium margaritaceum* genome: Hallmarks of the origins of land plants. *Cell*, 181, 1097–1111. <https://doi.org/10.1016/j.cell.2020.04.019>
- Kaewthai, N., Gendre, D., Eklöf, J. M., Ibatullin, F. M., Ezcurra, I., Bhalarao, R. P., & Brumer, H. (2013). Group III-A XTH genes of *Arabidopsis* encode predominant xyloglucan endohydrolases that are dispensable for normal growth. *Plant Physiology*, 161, 440–454. <https://doi.org/10.1104/pp.112.207308>
- Kolosova, N., Miller, B., Ralph, S., Ellis, B. E., Douglas, C., Ritland, K., & Bohlmann, J. (2004). Isolation of high-quality RNA from gymnosperm and angiosperm trees. *BioTechniques*, 36, 821–824. <https://doi.org/10.2144/043655T06>
- Kozlova, L. V., Nazipova, A. R., Gorshkov, O. V., Petrova, A. A., & Gorshkova, T. A. (2020). Elongating maize root: zone-specific combinations of polysaccharides from type I and type II primary cell walls. *Scientific Reports*, 10, 10956. <https://doi.org/10.1038/s41598-020-67782-0>
- McCown, B. H., & Lloyd, G. (1981). Woody plant medium (WPM) - a revised mineral formulation for micro-culture of woody plant species. *HortScience*, 16, 453.
- McGregor, N., Yin, V., Tung, C. C., Van Petegem, F., & Brumer, H. (2017). Crystallographic insight into the evolutionary origins of xyloglucan endotransglycosylases and endohydrolases. *Plant Journal*, 89, 651–670. <https://doi.org/10.1111/tpj.13421>
- Mellerowicz, E. J., Immerzeel, P., & Hayashi, T. (2008). Xyloglucan: The Molecular Muscle of Trees. *Annals of Botany*, 102, 659–665. <https://doi.org/10.1093/aob/mcn170>
- Michel, G., Chantalat, L., Duee, E., Barbeyron, T., Henrissat, B., Kloareg, B., & Dideberg, O. (2001). The κ -carrageenase of *P. carrageenovora* features a tunnel-shaped active site: A novel insight in the evolution of clan-B glycoside hydrolases. *Structure*, 9, 513–525. [https://doi.org/10.1016/S0969-2126\(01\)00612-8](https://doi.org/10.1016/S0969-2126(01)00612-8)
- Mottiar, Y., Karlen, S. D., Goacher, R. E., Ralph, J., & Mansfield, S. D. (2022). Metabolic engineering of p-hydroxybenzoate in poplar lignin. *Plant Biotechnol J*, in press., 21, 176–188. <https://doi.org/10.1111/pbi.13935>
- Obel, N., Erben, V., Schwarz, T., Kühnel, S., Fodor, A., & Pauly, M. (2009). Microanalysis of plant cell wall polysaccharides. *Molecular Plant*, 2, 922–932. <https://doi.org/10.1093/mp/ssp046>
- Pauly, M., Andersen, L. N., Kauppinen, S., Kofod, L. V., York, W. S., Albersheim, P., & Darvill, A. (1999). A xyloglucan-specific endo- β -1,4-glucanase from *Aspergillus aculeatus*: Expression cloning in yeast, purification and characterization of the recombinant enzyme. *Glycobiology*, 9, 93–100. <https://doi.org/10.1093/glycob/9.1.93>
- Perrot, T., Pauly, M., & Ramirez, V. (2022). Emerging roles of beta-glucanases in plant development and adaptive responses. *Plants-Basel*, 11, 22.
- Pinard, D., Mizrachi, E., Hefer, C. A., Kersting, A. R., Joubert, F., Douglas, C. J., Mansfield, S. D., & Myburg, A. A. (2015). Comparative analysis of plant carbohydrate active enzymes and their role in xylogenesis. *BMC Genomics*, 16, 402. <https://doi.org/10.1186/s12864-015-1571-8>
- Popper, Z. A., Michel, G., Hervé, C., Domozych, D. S., Willats, W. G., Tuohy, M. G., Kloareg, B., & Stengel, D. B. (2011). Evolution and diversity of plant cell walls: from algae to flowering plants. *Annual Review of Plant Biology*, 62, 567–590. <https://doi.org/10.1146/annurev-arplant-042110-103809>
- Preibisch, S., Saalfeld, S., & Tomancak, P. (2009). Globally optimal stitching of tiled 3D microscopic image acquisitions. *Bioinformatics*, 25, 1463–1465. <https://doi.org/10.1093/bioinformatics/btp184>
- Ruiz-May, E., & Rose, J. K. (2013). Progress toward the tomato fruit cell wall proteome. *Frontiers in Plant Science*, 4, 159. <https://doi.org/10.3389/fpls.2013.00159>
- Scheller, H. V., & Ulvskov, P. (2010). Hemicelluloses. *Annual Review of Plant Biology*, 61, 263–289. <https://doi.org/10.1146/annurev-arplant-042809-112315>
- Schindelin, J., Arganda-Carreras, I., Frise, E., Kaynig, V., Longair, M., Pietzsch, T., Preibisch, S., Rueden, C., Saalfeld, S., Schmid, B., Tinevez, J. Y., White, D. J., Hartenstein, V., Eliceiri, K., Tomancak, P., & Cardona, A. (2012). Fiji: an open-source platform for biological-image analysis. *Nature Methods*, 9, 676–682. <https://doi.org/10.1038/nmeth.2019>
- Schultink, A., Liu, L., Zhu, L., & Pauly, M. (2014). Structural diversity and function of xyloglucan sidechain substituents. *Plants*, 3, 526–542. <https://doi.org/10.3390/plants3040526>
- Shinohara, N., & Nishitani, K. (2021). Cryogenian origin and subsequent diversification of the plant cell-wall enzyme XTH family. *Plant & Cell Physiology*, 62, 1874–1889. <https://doi.org/10.1093/pcp/pcab093>
- Sjödin, A., Street, N. R., Sandberg, G., Gustafsson, P., & Jansson, S. (2009). The *Populus* Genome Integrative Explorer (PopGenIE): a new resource for exploring the *Populus* genome. *New Phytologist*, 182, 1013–1025. <https://doi.org/10.1111/j.1469-8137.2009.02807.x>
- Snovida, S. I., Rak-Banville, J. M., & Perreault, H. (2008). On the use of DHB/aniline and DHB/N,N-dimethylaniline matrices for improved detection of carbohydrates: automated identification of oligosaccharides and quantitative analysis of sialylated glycans by MALDI-TOF mass spectrometry. *Journal of the American Society for Mass Spectrometry*, 19, 1138–1146. <https://doi.org/10.1016/j.jasms.2008.04.033>
- Somerville, C., Bauer, S., Brininstool, G., Facette, M., Hamann, T., Milne, J., Osborne, E., Paredes, A., Persson, S., Raab, T., Vorwerk, S., & Youngs, H. (2004). Toward a systems approach to understanding plant cell walls. *Science*, 306, 2206–2211. <https://doi.org/10.1126/science.1102765>
- Stratilova, B., Kozmon, S., Stratilova, E., & Hrmova, M. (2020). Plant xyloglucan xyloglucosyl transferases and the cell wall structure: Subtle but significant. *Molecules*, 25, 25. <https://doi.org/10.3390/molecules25235619>
- Sundell, D., Mannapperuma, C., Netotea, S., Delhomme, N., Lin, Y. C., Sjödin, A., Van de Peer, Y., Jansson, S., Hvidsten, T. R., & Street, N. R. (2015). The plant genome integrative explorer resource: PlantGenIE. *New Phytologist*, 208, 1149–1156. <https://doi.org/10.1111/nph.13557>
- Veličković, D., Ropartz, D., Guillon, F., Saulnier, L., & Rogniaux, H. (2014). New insights into the structural and spatial variability of cell-wall polysaccharides during wheat grain development, as revealed through MALDI mass spectrometry imaging. *Journal of Experimental Botany*, 65, 2079–2091. <https://doi.org/10.1093/jxb/eru065>
- Viborg, A. H., Terrapon, N., Lombard, V., Michel, G., Czjzek, M., Henrissat, B., & Brumer, H. (2019). A subfamily roadmap of the evolutionarily diverse glycoside hydrolase family 16 (GH16). *Journal of Biological Chemistry*, 294, 15973–15986. <https://doi.org/10.1074/jbc.RA119.010619>
- Winter, D., Vinegar, B., Nahal, H., Ammar, R., Wilson, G. V., & Provart, N. J. (2007). An “electronic fluorescent pictograph” browser for exploring and analyzing large-scale biological data sets. *PLoS ONE*, 2, 12. <https://doi.org/10.1371/journal.pone.0000718>
- Wise, A. A., Liu, Z., & Binns, A. N. (2006). Three methods for the introduction of foreign DNA into *Agrobacterium*. *Methods in Molecular Biology*, 343, 43–53.



- Yokoyama, R., Uwagaki, Y., Sasaki, H., Harada, T., Hiwatashi, Y., Hasebe, M., & Nishitani, K. (2010). Biological implications of the occurrence of 32 members of the XTH (xyloglucan endotransglucosylase/hydrolase) family of proteins in the bryophyte *Physcomitrella patens*. *Plant Journal*, *64*, 645–656. <https://doi.org/10.1111/j.1365-313X.2010.04351.x>
- Zachgo, S., Perbal, M. C., Saedler, H., & Schwarz-Sommer, Z. (2000). In situ analysis of RNA and protein expression in whole mounts facilitates detection of floral gene expression dynamics. *Plant Journal*, *23*, 697–702. <https://doi.org/10.1046/j.1365-313x.2000.00826.x>

SUPPORTING INFORMATION

Additional supporting information can be found online in the Supporting Information section at the end of this article.

How to cite this article: Behar, H., Mottiar, Y., Chandrasekhar, R., Grappadelli, A. C., Pauly, M., Samuels, A. L., Mansfield, S. D., & Brumer, H. (2023). *Populus* endo-glucanase 16 localizes to the cell walls of developing tissues. *Plant Direct*, *7*(2), e482. <https://doi.org/10.1002/pld3.482>